Miscible Blends of Cyclic Poly(oxyethylene) in Linear Polystyrene

Swati Singla and Haskell W. Beckham*

School of Polymer, Textile and Fiber Engineering, Georgia Institute of Technology, Atlanta, Georgia 30332-0295

Received February 13, 2008; Revised Manuscript Received November 4, 2008

ABSTRACT: Cyclic poly(oxyethylene) (POE) was prepared from hydroxyl-terminated linear POE with molecular weights from 400 to 1500 g/mol using a dilute-solution end-coupling route. These cyclic and linear POEs were solution-mixed with linear polystyrene (PS, 15 kg/mol) to prepare binary blends with POE concentrations from 1.5 to 40 wt %. To assess the effect of end groups, PS was also blended with methoxyl-terminated linear POE with molecular weights from 500 to 2000 g/mol. Thermal analysis was conducted using differential scanning calorimetry to measure the glass transitions (T_g) in the blends. Using the Fox equation and the blend T_g, we estimated the fraction of POE dissolved into the PS. Across the entire concentration and molecular weight ranges studied, cyclic POE exhibited significantly enhanced miscibility compared to the linear POEs. For the smallest POE additives at concentrations ≤10 wt %, completely miscible blends were formed with cyclic POE, partially miscible blends were formed with the methoxyl-terminated linear POE, and the hydroxyl-terminated linear POE was completely immiscible. ^{1}H solid-state NMR spectroscopy was used to examine the POE dynamics and domain sizes in these dynamically asymmetric blends. In the completely miscible blends, the dissolved POE is characterized by typical smallest diameters of 1−1.5 nm and exhibits reduced segmental mobilities compared to pure POE. In the partially miscible blends, two dynamically distinct POE domains are detected, representing the dissolved POE and phase-separated POE. The phase-separated POE exhibits higher segmental mobilities in larger domains (>∼20 nm).

Introduction

Polystyrene and poly(oxyethylene) (POE) are not miscible over wide ranges of temperature, composition, and molecular weight.[1−3] Miscibility can be enhanced by using styrene copolymers containing functional groups that hydrogen bond to the POE. Example comonomers include hydroxystyrenes,[4] acrylic acid,[5] or methacrylic acid.[6] The use of such functionalized polymers to reduce the enthalpy of mixing is a common method for compatibilization of immiscible polymer blends. Other methods include (1) addition of copolymer additives[7] and (2) in situ generation of interfacially active polymers by (a) using reactive components with complementary functional groups[8] or (b) solid-state shear pulverization.[9] These techniques require either the addition of an extra component or its synthesis by chemical modification of one or more of the constituent polymers.

An alternative method for improving blend miscibility is to simply replace one of the linear components with a cyclic version of the same polymer. In 1986, Cates and Deutsch[10] reported some computational results on cyclic/linear blends in which they predicted "...it may be possible to find pairs of chemical species A, B such that linear chains of each species are incompatible ($\chi > 0$), but that rings of one species are compatible with linear chains of the other ($\chi < 0$)." Six years later, Santore, Han, and McKenna reported that cyclic polystyrene (PS) exhibited a slightly higher LCST (lower critical solution temperature) and was less mobile than linear PS in blends with linear poly(vinyl methyl ether) (PVME).[11] Since then, a few other examples have been reported:[12] cyclic poly(dimethylsiloxane) with linear poly(methylphenylsiloxane),[13] and cyclic polycarbonate with a number of linear amorphous polymers as evidenced by reduced calorimetric T_g's.[14,15]

Increased miscibility for cyclic/linear polymer blends as compared to linear/linear polymer blends can be explained by topological effects. If as-synthesized pure cyclic polymers are not concatenated or knotted, then these configurations remain unavailable to them in the solid state. This additional excluded volume due to topology leads to significantly reduced entropy for pure cyclic polymers. In contrast, there is no unavailable configurational space for linear/linear and cyclic/linear blends since they can interpenetrate freely. Therefore, mixing of cyclic/linear polymer blends can be thermodynamically favored due to the entropy gain involved when going from pure cycles to cyclic/linear blends.[15,16]

For polymers with sufficiently low molecular weights, miscibility is greatly affected by end groups. It has been shown that the χ parameter can be changed by using different end groups.[17,18] Thus, miscibility differences between cyclic/linear blends and linear/linear blends could be attributed to loss of the end groups. The earlier study on blends of PVME with cyclic PS employed 247 kg/mol cyclic PS, and thus end-group effects are not expected to play a major role there.[11] The study conducted by Nachlis et al.[15] focused on cyclic bisphenol A carbonate oligomers, for which loss of end groups might be expected to influence blend miscibility. However, the authors did not find a strong dependence of the χ parameter on the nature of the end groups and concluded that the difference between the χ values for cyclic/linear and linear/linear polymer blends was too large to be due to the chemical nature of the end groups.[15]

Cyclization as a route to miscible polymer blends is relatively unexplored. Because of the recent availability of a larger variety of cyclic polymers from new[19−21] and efficient[22,23] synthetic schemes, this method warrants further examination. In this contribution, we report that cyclic poly(oxyethylene) exhibits significant miscibility with linear polystyrene. We compared the miscibility of linear polystyrene with low-molecular-weight cyclic and linear poly(oxyethylene). The linear POE is terminated with hydroxyl end groups. To assess the effect of losing these hydroxyl end groups on blend miscibility, we also examined blends of linear PS with linear poly(ethylene glycol) dimethyl ether, which is a methoxyl-terminated linear POE. Miscibility was assessed by thermal analysis using differential scanning calorimetry and by solid-state NMR measurements.

* Corresponding author: e-mail beckham@gatech.edu.

10.1021/ma800327c CCC: $40.75
Published on Web 11/24/2008

Solid-state NMR was used to characterize the relative mobility of the POE component in the binary blends and also the POE domain sizes via spin-diffusion studies.

Experimental Section

Materials. Unless stated otherwise, all starting materials and solvents were purchased from Aldrich and used without further purification.

Poly(oxyethylene). α-Hydro-ω-hydroxypoly(oxyethylene) (lPOE, $M_n \sim 400$, 600, 900, and 1500 g/mol) and α-methyl-ω-methoxypoly(oxyethylene) (lPDME, $M_n \sim 500$, 1000, and 2000 g/mol) were dried under vacuum for a period of days. Cyclic POE (cPOE) was synthesized from lPOE and purified according to previously reported procedures.[23] Yields for each molecular weight were 63% (400 g/mol), 68% (600 g/mol), 73% (900 g/mol), and 80% (1500 g/mol). Each cyclic POE sample is 100% free of linear byproducts, according to NMR and MALDI-TOF mass spectrometry, and exhibits GPC polydispersities of ≤1.1.[23] In the text, the different POEs are signified by an acronym and subscripted molecular weight. For example, $cPOE_{400}$ is the 400 g/mol cyclic poly(oxyethylene).

Polystyrene. Styrene (99%) was passed through an inhibitor removal column and then polymerized in toluene (20% styrene w/w) using azobis(isobutyronitrile) (1% w/w based on styrene). The resulting product was dissolved in CH_2Cl_2 and precipitated into methanol thrice to yield polystyrene (PS): yield = 60%; $M_n = 15$ kg/mol, $M_w = 20$ kg/mol by GPC, $T_g = 94$ °C by DSC (10 °C/min).

POE/PS Blends. Blends of polystyrene and POE were prepared by solution mixing in toluene (10% solids w/v). Both polymers of a given blend composition were dissolved in toluene separately, mixed, and sonicated for 15 min. The clear solutions were cast onto Petri dishes and allowed to sit overnight at room temperature. The dried films were scraped off, dried under vacuum at 60 °C for 48 h, and then annealed under vacuum at 120 °C for 24 h. The annealed samples were allowed to slowly cool back to room temperature over a period of hours and then stored at room temperature in a desiccator under vacuum. The final blend concentration was confirmed by quantitative ^{1}H NMR in $CDCl_3$. Five different blend concentrations were investigated: 1.5, 4.5, 10, 25 and 40% (w/w POE in PS).

Instrumentation and Methods. Solution-state ^{1}H NMR spectra were measured with a Bruker DRX-500 spectrometer on 1 wt % solutions in DMSO-d_6 or $CDCl_3$. A recycle delay of 10 s was used to ensure quantitative analysis.

Differential scanning calorimetry (DSC) was conducted on a SEIKO 220C under nitrogen. Samples (10−30 mg) were sealed in aluminum pans. The power and temperature scales of the calorimeter were calibrated against the enthalpies of fusion and melting temperature of pure indium and tin. All thermograms were baseline-corrected by subtracting the thermogram for an empty aluminum pan, measured under the same conditions. A typical experiment consisted of fast cooling to −150 °C, slow heating to 150 °C, hold at 150 °C for 10 min, slow cooling to −150 °C, hold at −150 °C for 5 min, and slow heating to 150 °C. The slow heating and cooling rate was 10 °C/min. The thermograms reported here were obtained from the second heating. Values of the enthalpies of fusion ($\Delta_{fus}H$) were obtained from peak areas. Melting temperatures (T_m) were obtained from the peak maxima. The percentage crystallinity was calculated using a fixed value for the melting enthalpy, 200 J/g, reported for a 100% crystalline hydroxyl-terminated POE.[24]

Solid-state NMR measurements were carried out on a Bruker DSX-300 spectrometer using a Bruker double-resonance MAS probe head. Unless stated otherwise, spinning speeds of 5 kHz were used, and spectra were collected at room temperature (24 °C). ^{1}H wide-line spectra were collected on static samples or under MAS using a 5 s recycle delay, a 5 μs ^{1}H 90°pulse length, and 8−32 scans.

Spin-diffusion experiments, also called dipolar magnetization transfer, were conducted under MAS using the dipolar filter sequence.[25] The experiment begins by selection of the mobile-phase ^{1}H magnetization using a dipolar filter consisting of 12 π/2 pulses, each separated by a delay time, τ. The filter sequence can be cycled n times. Selection is followed by a variable mixing time (t_m) to allow diffusion of the mobile-phase magnetization into the rigid phase and then detection of the ^{1}H signal or, by insertion of a cross-polarization sequence, the ^{13}C signal. For sufficiently long mixing times, the magnetization is equilibrated across the sample. If the filter is adjusted properly (by appropriate settings of τ and n), the T_1-corrected and normalized (vide infra) magnetization at equilibrium corresponds to the stoichiometric mobile-phase ^{1}H fraction in the sample. The filter strength was thus optimized with $\tau = 10$ μs and $n = 5$. Pulse lengths were 5 μs for the ^{1}H 90° and 10 μs for the ^{1}H 180°. The mixing time (t_m) was incremented from 100 μs to 1.6 s; 32 scans, each separated by a 5 s recycle delay, were collected for every mixing time. Spin−lattice relaxation occurs during the mixing time and leads to signal decay. To correct for this, the experiment was conducted a second time for each sample but with the selection filter removed ($n = 0$). After normalization to $t_m = 100$ μs, the ratio of signal intensity with selection (I_{POE}) to signal intensity without selection ($I_{POE,0}$) was plotted versus $\sqrt{t_m}$ to obtain the spin-diffusion decay curve.

We used the initial-rate approximation to estimate the POE domain sizes from the experimental spin-diffusion decay curves.[26,27] In general, small domains are characterized by a more rapid decay than are large domains. A straight line fitted to the initial part of the spin-diffusion decay curve will intercept the x-axis at lower values for small domains than for larger domains. Such initial-rate data may be used to estimate the domain sizes:

$$d_{POE} = \frac{2\varepsilon}{\sqrt{\pi}}\sqrt{D_{eff}t_m^*} \quad (1)$$

where d_{POE} is the POE domain size ("typical smallest diameter"), ε is the dimensionality of the spin diffusion (e.g., $\varepsilon = 3$ for three-dimensional, $\varepsilon = 2$ for 2D, and $\varepsilon = 1$ for 1D), D_{eff} is the effective spin-diffusion coefficient, and $\sqrt{t_m^*}$ is the x-axis intercept of a straight line fitted to the initial part of the spin-diffusion decay curve. The D_{eff} is an average of the rigid-phase (i.e., PS) and mobile-phase (i.e., POE) spin-diffusion coefficients:[27,28]

$$\sqrt{D_{eff}} = \frac{\sqrt{D_{PS}}\sqrt{D_{POE}}}{(\sqrt{D_{PS}} + \sqrt{D_{POE}})/2} \quad (2)$$

A value of 0.8 ± 0.2 nm^2/ms was used for D_{PS}.[25] The D_{POE} was computed from the spin−spin relaxation time (T_2) of the POE-phase magnetization using some empirically established relations determined on static samples.[28] Although our samples were measured under MAS, the reported calibration curve is expected to be valid since MAS reduces both spin-diffusion and spin−spin relaxation rates by averaging of dipolar interactions. The POE T_2's were measured for each blend sample under MAS using the dipolar selection filter immediately followed by a Hahn echo sequence.[29] The mixing time was fixed at 10 μs, and τ was incremented from 20 μs to 6 ms. The measured echo maxima were normalized and then plotted as a function of 2τ to provide the echo decay curves which were fitted to determine the POE T_2's. D_{POE} values for all blends are listed in Table 2.

Results and Discussion

DSC data for the pure POE components are summarized in Table 1. All three versions of the POE (hydroxyl-terminated linear, methoxyl-terminated linear, and cyclic) are semicrystalline and exhibit melting endotherms in their DSC traces. Glass transitions (T_g) are observed for the smallest POEs at −72 °C ($cPOE_{400}$ and $lPOE_{400}$) and at −70 °C ($lPDME_{500}$). With the exception of the $cPOE_{600}$ ($T_g = -68$ °C), all other POE samples were so highly crystalline that it was difficult to detect the glass transition. Repeated attempts to observe T_g's by quenching samples from the melt were unsuccessful. For the same molecular weight, the cyclic POEs exhibit lower melting

Table 1. Thermal Data for Hydroxyl-Terminated Linear POE (lPOE), Methoxyl-Terminated Linear POE (lPDME), and Cyclic POE (cPOE)

sample	T_g (°C)[a]	T_m (°C)[a]	$\Delta_{fus}H$ (J/g)[a]	% crystallinity
$lPOE_{400}$	−72	4	91	46
$lPOE_{600}$	*b*	21	128	64
$lPOE_{900}$	*b*	37	143	71
$lPOE_{1500}$	*b*	50 (47[c])	172 (165[c])	86
$cPOE_{400}$	−72	−7	27	13
$cPOE_{600}$	−68	7	44	22
$cPOE_{900}$	*b*	26	107	54
$cPOE_{1500}$	*b*	48 (47[c])	136 (140[c])	68
$lPDME_{500}$	−70	15	116	58
$lPDME_{1000}$	*b*	39	130	64
$lPDME_{2000}$	*b*	61	190	95

[a] Errors: $T_g \pm 2$ °C, T_m (lPOE) ± 2 °C, T_m (cPOE) ± 5 °C, $\Delta_{fus}H \pm 10$ J/g. [b] T_g was difficult to detect with DSC. [c] T_m and $\Delta_{fus}H$ values taken from the literature.[31]

temperatures (T_m), lower melting enthalpies ($\Delta_{fus}H$), and therefore lower crystallinities than the linear POEs, consistent with the literature.[30−33]

DSC thermograms are shown in Figure 1 for linear polystyrene and its blends with $lPOE_{400}$, $lPDME_{500}$, and $cPOE_{400}$ at POE concentrations of 10 wt %. The PS T_g (94 °C) is apparently depressed for each of the blend samples, indicating that some fraction of each of these low-molecular-weight POE additives dissolves into the PS. The magnitude of the depression occurs in the following order: lPOE (87 °C) < lPDME (79 °C) < cPOE (66 °C), meaning more cPOE dissolves into PS than either linear POE. In the DSC trace of the $lPOE_{400}$/PS blend, the appearance of the lPOE melting endotherm, very close to that of the pure $lPOE_{400}$, reveals the presence of a large separate lPOE phase. A separate T_g for $lPOE_{400}$ is not discernible in this sample. In contrast, separate POE T_g's and no melting endotherms are observed for the blends with $lPDME_{500}$ and $cPOE_{400}$. Note, however, that the POE T_g's are only seen when the *y*-axis is expanded and appear at significantly higher temperatures (0 °C) than the T_g's for the pure POE components (∼−70 °C). The dissolved POE in these blends is characterized by slower segmental motions than in pure POE, consistent with POE in miscible blends with poly(methyl methacrylate).[34−37]

Historically, the presence of two calorimetric T_g's in polymer blends was taken as an indicator of immiscibility, at least to some degree. However, NMR studies as early as 1990 by Miller et al.[38] showed that a polymer blend could be intimately mixed but still have each of its components exhibit distinct dynamics. While the blend that they studied, polyisoprene/poly(vinylethylene), did exhibit a single albeit broad calorimetric T_g, they pointed out that "in principle even distinct glass transition temperatures" are "not inconsistent with thermodynamic miscibility".[38] Since that time, numerous studies have confirmed that individual components of apparently miscible polymer blends do indeed exhibit distinct dynamics.[39,40] The question really is, why are not separate T_g's observed for the individual components of miscible polymer blends? This has been recently and nicely addressed by Lodge et al.[41] In general, for miscible blends with widely separated T_g's, it is easier to observe the two calorimetric T_g's. One particularly relevant and widely studied case is the miscible blend of POE and poly(methyl methacrylate) (PMMA), for which the pure-component T_g separation is >180 K. The literature contains studies that report either a single T_g[42] or two T_g's[43,44] from DSC thermograms of POE/PMMA blends. As shown in Figure 1 and mentioned above for the POE/PS blends studied here, it would have been easy to overlook these elevated POE T_g's.

Separate component T_g's in miscible polymer blends are predicted using the Lodge−McLeish model. According to this model, effective component T_g's exist as a consequence of the local environment of a given component being rich in that component due to chain connectivity. This leads to an effective T_g of the low-T_g component being depressed and an effective T_g of the high-T_g component being elevated relative to the blend average T_g. The relevant volume (V) over which this self-concentration effect takes place is calculated using the Kuhn length (l_k): $V \sim l_k^3$; the fraction of one Kuhn's length of polymer actually occupying this volume is called the self-concentration, ϕ_{self}. These self-concentrations can then be used to compute effective weight fractions. If these effective weight fractions are used in the Fox equation (note that this approach is not required by the Lodge−McLeish model), effective T_g's can be calculated for each component of a blend. The Kuhn length can be estimated from the characteristic ratio, $l_k = C_\infty l$, where l is the length of the average backbone bond. Characteristic ratios of 3.8 to 6.7 have been reported for POE, with most ranging from about 4 to 5.[45−47]

Using a Kuhn length for POE computed from a characteristic ratio of 5,[48] and the component T_g's measured for our pure POE and PS, the Lodge−McLeish model predicts a self-concentration of 0.29, from which we calculate an effective T_g of 9 °C for the POE in the 10 wt % blend with PS. This is close to but slightly higher than the experimentally observed value of 0 °C (see Figure 1). We used $C_\infty = 5$ since this value was measured for POE in dilute nonaqueous solvents and therefore does not incorporate condensed phase effects.[48] The observed POE T_g is not related to topology, as the cyclic POE and methoxyl-terminated linear POE (lPDME) both exhibit the T_g around 0 °C in their blends with PS (see Figure 1). A separate elevated POE T_g was observed between −10 and 0 °C for all cPOE/PS blends up to 10 wt % and some of the PS/lPDME blends. For the 4.5 wt % blends, the Lodge−McLeish model predicts an effective POE T_g of 17 °C, which is higher than the experimentally observed elevated POE T_g's (−10 to 0 °C).

For the PS, a Lodge−McLeish self-concentration of 0.15 was calculated which leads to an effective T_g of 73 °C for the 10 wt % blends. The experimentally observed T_g occurs at 66 °C in the cPOE/PS blend. Thus, the Lodge−McLeish effective T_g's are higher than both T_g's in the DSC thermogram of the 10 wt % cPOE/PS blend shown in Figure 1. Using DSC, separate component T_g's have been detected in miscible polymer blends and quantitatively matched with the effective T_g's predicted by the Lodge−McLeish model.[49] However, these blends exhibited single broad glass transitions in their heat capacity curves; two peaks were only revealed after taking the derivative of the heat capacity curves.[49] The two T_g's observed for the POE/PS blends are not the effective T_g's predicted by the Lodge−McLeish model. The elevated POE T_g observed in Figure 1 is more likely a manifestation of restricted segmental dynamics of the POE confined in the relatively static PS matrix. Dynamic confinement effects have recently been observed for dilute concentrations of POE in PMMA,[50] poly(vinyl acetate),[51] and poly(ether sulfone)[52] near and below the blend T_g. The two T_g's observed in Figure 1 are best described as the average blend T_g (the stronger transition at higher temperatures) and the confined POE transition (the weaker transition at lower temperatures), both of which should be and are lower than the effective component T_g's predicted by the Lodge−McLeish model.[53]

The blend T_g observed in DSC for the $cPOE_{400}$/PS blend (see Figure 1) is perfectly described by the Fox equation:[54]

$$\frac{1}{T_{g,blend}} = \frac{w_{PS}}{T_{g,PS}} + \frac{w_{POE}}{T_{g,POE}} \quad (3)$$

where w_{PS} and w_{POE} are the weight fractions of PS and POE in the blend and $T_{g,PS}$ and $T_{g,POE}$ are the glass transitions of the two homopolymers. Using the Fox equation and the blend T_g,

Table 2. Domain Sizes Obtained from NMR Spin-Diffusion Experiments for Blends of PS with Cyclic POE (cPOE), Methoxyl-Terminated Linear POE (lPDME), or Hydroxyl-Terminated Linear POE (lPOE)

POE component in blend with PS	POE content (% w/w)	D_{POE} (nm^2/ms)	d_{POE} (nm) dissolved[a]	d_{POE} (nm) phase-separated[b]	miscibility: complete (c), partial (p), not (n)
$cPOE_{400}$	1.5	0.07	1.1		c
	4.5	0.07	1.3		c
	10	0.07	1.5		c
	25	0.07, 0.01	5	~49	p
	40	0.01, 0.01	8	~62	p
$cPOE_{600}$	4.5	0.07, 0.01	1.4	~130	p
$cPOE_{900}$	4.5	0.07, 0.01	1.6	~130	p
$cPOE_{1.5K}$	4.5	0.01, 0.01	3	~26	p
$lPDME_{500}$	1.5	0.07, 0.01	2	~23	p
	4.5	0.07, 0.01	3	~35	p
	10	0.07, 0.01	3	~22	p
	25	0.007		~100	n
	40	0.007		~100	n
$lPDME_{1K}$	4.5	0.01, 0.01	5	~45	p
$lPDME_{2K}$	4.5	0.007		~100	n
$lPOE_{400}$	1.5−40	0.007		~100	n
$lPOE_{600}$	4.5	0.007		~100	n
$lPOE_{900}$	4.5	0.007		~100	n
$lPOE_{1.5K}$	4.5	0.007		~100	n

[a] Dissolved POE domain size computed using $\varepsilon = 1$. [b] Phase-separated POE domain size computed using $\varepsilon = 3$.

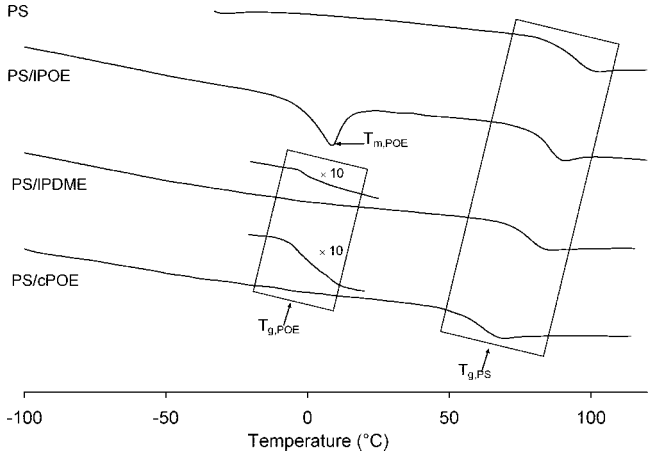

Figure 1. DSC thermograms for polystyrene (PS) and its blends (10 wt %) with hydroxyl-terminated linear poly(oxyethylene) (lPOE, 400 g/mol), methoxyl-terminated linear POE (lPDME, 500 g/mol), and cyclic POE (cPOE, 400 g/mol).

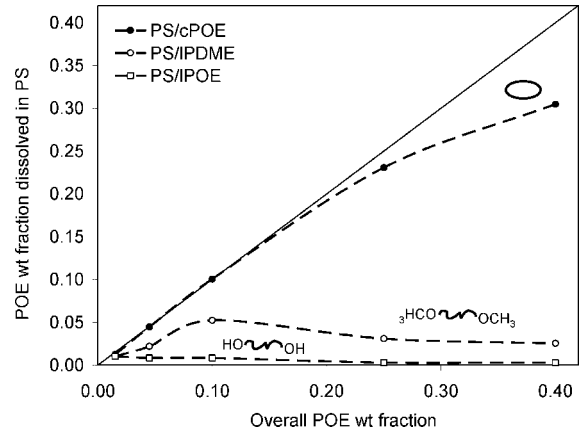

Figure 2. Weight fraction of POE incorporated into PS blended with cyclic POE (●, cPOE, 400 g/mol), methoxyl-terminated linear POE (○, lPDME, 500 g/mol), or hydroxyl-terminated linear POE (□, lPOE, 400 g/mol) as a function of the overall POE weight fraction. The weight fraction incorporated into the PS-rich phase was determined using the blend T_g from DSC and the Fox equation (eq 3). For the cPOE in PS, the blend T_g's are 90, 81, 66, 35, and 20 °C for 1.5, 4.5, 10, 25, and 40 wt %, respectively. The solid line represents complete dissolution of the POE into the PS. The dashed lines are drawn as guides to distinguish the behavior of the three different POE additives.

the weight fraction of POE that dissolves into the PS, w_{POE}, can be calculated since $w_{PS} = 1 - w_{POE}$. Figure 2 shows the weight fraction of $cPOE_{400}$, $lPDME_{500}$, and $lPOE_{400}$ incorporated into polystyrene as a function of the overall POE weight fraction. Across the entire concentration range, cPOE exhibits significantly higher miscibility than lPDME, and lPOE is immiscible in PS. At 10 wt %, for which the DSC data are shown in Figure 1, the entire cPOE fraction, about half of the lPDME fraction, and very little of the lPOE fraction mix into the PS phase according to the Fox equation. For the $lPDME_{500}$/PS blend, 10 wt % seems to be a critical composition as the fraction of $lPDME_{500}$ incorporated into the PS-rich phase decreases for higher POE concentrations. It is known that replacing hydroxyl with methoxyl end groups in POE decreases the upper critical solution temperature of its blends with PS, which can increase miscibility for a given temperature.[55] However, even when both components are low molecular weight (2−3 kg/mol), the phase boundary is near 100 °C for a lPDME/PS blend containing 10% lPDME.[55] The DSC data of Figures 1 and 2 show that both topology and end groups affect the miscibility behavior for POE/PS blends; topological effects are however greater than the end-group effects. Even up to 40 wt % overall POE in the blend, as much as 30 wt % of the cyclic POE_{400} is incorporated in the PS phase, while less than 3% of the linear POE additives are miscible.

The effect of POE molecular weight on blend compatibility was also studied by DSC. Figure 3 shows the weight fraction of POE incorporated into the PS phase as a function of POE molecular weight for a POE blend concentration of 4.5 wt %. Across all molecular weights, cPOE exhibits significantly higher miscibility than the linear POEs. The lPDME again displays an intermediate behavior between cPOE and lPOE. The lPDME fraction incorporated into PS seems to decrease much more with chain length, with the trend suggesting that molecular weights >2 kg/mol might be as strongly phase-separated as the lPOE. This behavior is consistent with reduced end-group effects for increasing molecular weight. The cyclic POE_{400} appears to be entirely incorporated into the PS at this concentration, but not for higher molecular weights. However, the cPOE weight fraction incorporated into the PS-rich phase does not decrease significantly from about 600 to 1500 g/mol. Comparing the POE

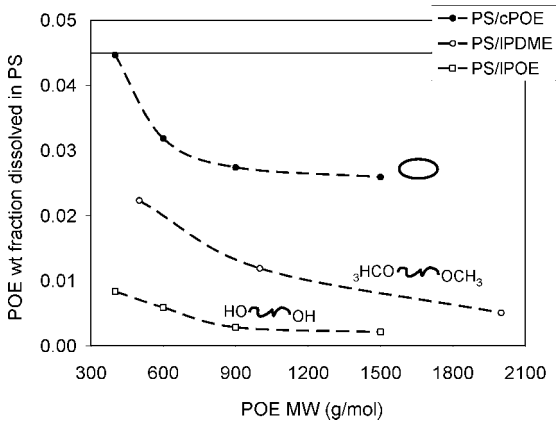

Figure 3. Weight fraction of POE incorporated into PS blended with cyclic POE (●, cPOE), methoxyl-terminated linear POE (○, lPDME), or hydroxyl-terminated linear POE (□, lPOE) as a function of the POE molecular weight. The weight fraction incorporated into the PS-rich phase was determined using the blend T_g from DSC and the Fox equation (eq 3). The solid line represents complete dissolution of the POE into the PS at the overall weight fraction of 4.5%. The dashed lines are drawn as guides to distinguish the behavior of the three different POE additives.

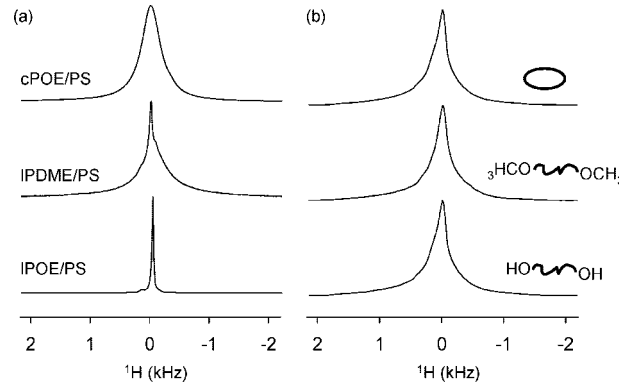

Figure 4. (a) ^{1}H solid-state NMR line shapes for blends of PS with 10 wt % of (from top to bottom) cyclic POE (cPOE, 400 g/mol), methoxyl-terminated linear POE (lPDME, 500 g/mol), or hydroxyl-terminated linear POE (lPOE, 400 g/mol). Spectra, collected at room temperature while magic-angle spinning (MAS) at 5 kHz, are expanded to display the narrow POE component only; the underlying broad component due to PS is not shown. The spectra are scaled to the same intensity. (b) ^{1}H solid-state NMR line shapes for (from top to bottom) cPOE$_{400}$, lPDME$_{500}$, and lPOE$_{400}$. These POE samples are liquids at room temperature so spectra were collected without MAS. The blend samples were measured under MAS because the narrow POE component for the cPOE and lPDME blends are only resolved under MAS.

additives with the highest molecular weights again suggests that topological effects dominate end-group effects on blend miscibility.

Figures 2 and 3 display miscibility information obtained from DSC measurements on the POE/PS blends, based on the assumption that the Fox equation applies to these blends. While DSC is sometimes used to map out phase diagrams, the procedure typically involves quenching a melted sample to a defined annealing temperature followed by scanning to probe the existence of one or two T_g's. As described in the Experimental Section, each POE/PS blend sample was held at 150 °C for 10 min, slowly cooled to −150 °C, and then slowly heated to measure the blend T_g, from which the weight fraction of dissolved POE was determined using eq 3. Because of the slow cooling step after annealing the samples at 150 °C, the sample temperatures are ill-defined prior to scanning to probe the location of the T_g (or T_g's). Thus, Figures 2 and 3 cannot be directly converted into conventional phase diagrams.

POE Dynamics from Solid-State NMR Line Shapes. The blend dynamics in the kilohertz regime were examined with solid-state ^{1}H NMR spectroscopy. The ^{1}H solid-state NMR spectra of all the samples consist of a narrow peak due to the mobile POE superimposed on a very broad peak due to the rigid PS. Spectra, expanded to display only the POE region, are shown in Figure 4a for blends of PS with cPOE$_{400}$, lPDME$_{500}$, and lPOE$_{400}$ for POE concentrations of 10 wt %. The line width for cPOE$_{400}$ ($\Delta\nu_{1/2} \sim 400$ Hz) is 10 times broader than that of lPOE$_{400}$ ($\Delta\nu_{1/2} \sim 40$ Hz), signifying considerably reduced mobility for cPOE$_{400}$ in the blends when compared to lPOE$_{400}$. The lPDME$_{500}$ peak in its PS blend consists of a narrow line superimposed on a broader component, suggesting two different dynamic regimes for lPDME$_{500}$ in the blends. Using two line shapes with widths characteristic of the more rigid cPOE$_{400}$ and mobile lPOE$_{400}$, the lPDME$_{500}$ peak can be fitted, revealing that about 60% of the lPDME$_{500}$ exists in a more rigid environment while about 40% exists as a mobile phase. Close observation of the two-component lPDME/PS line shape in Figure 4a reveals the narrow component to be slightly downfield from the rigid component. This fact, coupled with the relative fractions of the two components obtained by fitting, rule out the likelihood that the narrow component is simply due to the methoxyl end groups of the lPDME. The broad lPDME component does not correspond to crystalline lPDME that has phase separated in the blend. The DSC thermogram of the lPDME$_{500}$/PS blend in Figure 1 does not contain a melting endotherm.

The reduction in mobility for cPOE$_{400}$ and a portion of the lPDME$_{500}$ as compared to lPOE$_{400}$ in their blends with PS could be due to differences in (1) intrinsic mobilities and (2) local environments related to miscibility. As shown in Figure 4b, the ^{1}H line shapes of pure cPOE$_{400}$, lPDME$_{500}$, and lPOE$_{400}$ are nearly identical, signifying no differences in intrinsic mobilities in the kilohertz regime. Thus, the mobility reduction observed in Figure 4a for the cPOE$_{400}$ and a portion of the lPDME$_{500}$ in their blends with PS is attributed to enhanced miscibility, and therefore more intimate contact, with the rigid PS segments. Based strictly on the ^{1}H line widths, cPOE$_{400}$ is the most miscible, lPOE$_{400}$ is the least miscible, and lPDME$_{500}$ exhibits an intermediate behavior between the two, that is, partially miscible. These results are consistent with solid-state ^{13}C NMR line shape studies (data not shown), the DSC results shown in Figures 1 and 2, and with literature reports that POE segmental dynamics are reduced (compared to pure POE) in miscible POE/PMMA blends.[34−37]

The effect of POE concentration and molecular weight on the POE mobility in the blends was also examined with ^{1}H solid-state NMR. Across the entire concentration range, the ^{1}H line shapes for cPOE$_{400}$ are much broader than those of lPOE$_{400}$, consistent with the enhanced miscibility of cPOE observed in Figure 2. Indeed, as the fraction of cPOE$_{400}$ incorporated into the PS-rich phase deviates from the full-dissolution line of Figure 2, the cPOE line shapes for the 25 and 40 wt % blends exhibit a slight narrowing. However, they are still 20 times broader than the lPOE$_{400}$ line shapes, which remain narrow from 1.5 to 40 wt %. The lPDME$_{500}$ line shape consists of a cPOE-like rigid component and lPOE-like mobile component. The relative ratio of these two components is approximately equal up to 10 wt %, above which the rigid-component fraction decreases. At 40 wt %, the lPDME$_{500}$ line shape appears very much like the lPOE$_{400}$ line shape, consistent with a strongly phase-separated POE domain and the DSC results of Figure 2.

The ^{1}H line shapes for cPOE in its 4.5 wt % blends with PS were measured as a function of cPOE molecular weight. The line widths decrease with increasing size of cyclic POE: cPOE$_{400}$ = 400 Hz, cPOE$_{600}$ = 350 Hz, cPOE$_{900}$ = 300 Hz, and cPOE$_{1.5K}$

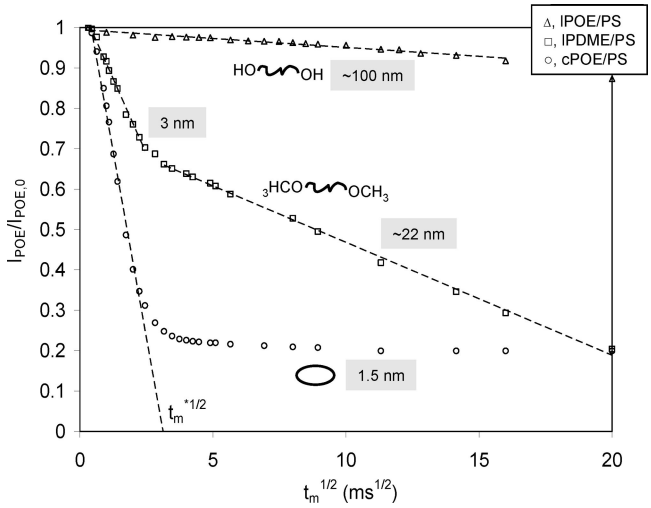

Figure 5. ^{1}H spin-diffusion curves for blends of PS with 10 wt % $lPOE_{400}$, $lPDME_{500}$, or $cPOE_{400}$. The normalized mobile-phase magnetization, $I_{POE}/I_{POE,0}$, is plotted as a function of the square root of the mixing time, $\sqrt{t_m}$. The dashed lines are fits to the initial part of each of the spin-diffusion curves that are extrapolated to the *x*-axis intercepts, $\sqrt{t_m^*}$, which are used in eq 1 to determine domain sizes. For the $lPDME_{500}$ curve, a second straight-line fit is shown for longer mixing times as this sample apparently consists of two separate POE domains. The computed POE domain sizes are located in the gray boxes adjacent to the associated decay curve.

= 150 Hz. The $cPOE_{1.5K}$ line shape is composed of two components, somewhat similar to the $lPDME_{500}$ line shape shown in Figure 4, indicating the presence of two different environments. This is consistent with the DSC results of Figure 3 which show that not all of the $cPOE_{1.5K}$ is mixed into the PS-rich phase of this binary blend. ^{1}H line shapes for the lPDME/PS and lPOE/PS blends were not analyzed as a function of POE molecular weight due to the contribution of POE crystallinity to the room-temperature ^{1}H line width. Crystallinity broadens the ^{1}H spectra, making it less straightforward to analyze line shapes in terms of miscibility alone. Although the $lPOE_{400}$ is certainly phase-separated and semicrystalline in its blend with PS (see Figure 1), the ^{1}H line shapes shown in Figure 4 were measured at room temperature, which is well above the T_m for the $lPOE_{400}$ (see Table 1).

POE Domain Sizes from Spin-Diffusion NMR. The mobility difference between the PS and POE allowed us to utilize dipolar magnetization transfer (i.e., spin diffusion) experiments to estimate the POE domain sizes. The dipolar filter was optimized to quantitatively select only the ^{1}H magnetization due to the POE. The broad component ($\Delta\nu_{1/2} \sim 30$ kHz) in the ^{1}H solid-state NMR spectra of the POE/PS binary blends is not present when the ^{1}H signal is measured immediately after application of the filter. The efficacy of the filter was further confirmed by measuring the filtered magnetization after cross-polarization to ^{13}C, which shows a single peak for POE (70.3 ppm) and no peaks for PS.

Here we use the broader meaning of the term "domain" to refer to the POE even if it is dissolved in the PS and forms a miscible blend. In this case the POE represents a domain that is distinguished from its surroundings by its dynamics. Even in pure amorphous polymers, dynamic heterogeneities that exist just above T_g have been characterized as "domains" and their sizes measured by spin-diffusion NMR.[56]

Figure 5 shows the spin-diffusion decay curves for binary blends of PS with $cPOE_{400}$, $lPDME_{500}$, and $lPOE_{400}$ for 10 wt % POE concentrations. The three blends show very different spin-diffusion behavior. The normalized mobile-phase magnetization ($I_{POE}/I_{POE,0}$) for the $cPOE_{400}$/PS blend monotonically decreases and reaches a plateau at an end value of ~0.2, corresponding to the stoichiometric POE ^{1}H fraction in the blend. A straight line is fitted to the initial part of this spin-diffusion decay curve (shown as a dashed line in Figure 5) and extrapolated to its intercept with the *x*-axis, where $I_{POE}/I_{POE,0} = 0$. This intercept yields the $\sqrt{t_m^*}$ value needed to compute the POE domain size using eq 1. According to eq 1, the domain size is directly proportional to a dimensionality factor, ε, that reflects the number of orthogonal directions for which a spin polarization gradient exists, and therefore spin diffusion is relevant. For microphase-separated block copolymers whose morphologies are known (e.g., from SAXS or TEM), it is straightforward to apply $\varepsilon = 1$ for lamellae, $\varepsilon = 2$ for cylinders, or $\varepsilon = 3$ for spheres. However, the appropriate ε value to use for miscible or partially miscible blends is not obvious without some independent information on the morphology.[57] The literature on spin-diffusion studies of polymer blends reports the use of $\varepsilon = 1$[58−62] and $\varepsilon = 2$.[63,64] For the dissolved POE, we used $\varepsilon = 1$ and assumed that the important polarization gradient is 1-dimensional for a POE chain segment in intimate contact with more rigid PS chain segments. For the phase-separated POE, we used $\varepsilon = 3$ although cylindrical or lamellar morphologies could also be justified for the blends containing higher POE concentrations (e.g., 25 and 40 wt %), which would lead to smaller computed domain sizes.

Based on the DSC (cf. Figure 2) and ^{1}H data (cf. Figure 4a), all of the $cPOE_{400}$ is dissolved into the PS at 10 wt % to yield single, dynamically hindered POE domains. The spin-diffusion curve for this sample shows a single rapid decay, similarly signifying a single POE domain. From the extrapolated initial decay, $\sqrt{t_m^*} = 3.2$ ms$^{1/2}$, from which eq 1 yields a d_{POE} of 1.5 nm using $\varepsilon = 1$. In contrast, the $lPOE_{400}$/PS spin-diffusion curve did not show much decay for the mixing times used, indicating large POE domains. The POE domain size in this case was estimated to be ~100 nm using the slope of the spin-diffusion curve. This is also consistent with the DSC (cf. Figure 2) and ^{1}H data (cf. Figure 4a) which show that most of the $lPOE_{400}$ is phase-separated from the PS at 10 wt % to yield single, dynamically mobile POE domains.

The spin-diffusion curve for the $lPDME_{500}$/PS blend exhibits a two-step decay, which we attribute to the dissolved POE (short-t_m fast decay) and the phase-separated POE (long-t_m slow decay). Such two-step spin-diffusion curves have been observed for emulsion-polymerized core−shell polymers in which only the short-t_m portion of the curve was analyzed to give the thickness of the interface.[65] Analysis of the long-t_m portion of such two-step spin-diffusion curves is not at all straightforward as it represents spin diffusion of magnetization that has originated from separate sources in typically unknown or perhaps irregular spatial arrangements. Applying the initial-rate approximation to the short-t_m portion of the two-step spin-diffusion curve shown in Figure 5 yielded 3 nm for the dissolved POE domains in the partially miscible $lPDME_{500}$/PS blends. This value was determined using $\varepsilon = 1$. As discussed above, using $\varepsilon = 1$ for dissolved POE that exists as isolated domains is done with some degree of ambiguity. However, in the partially miscible blends, instead of isolated domains, the dissolved POE could exist as the interface between the phase-separated POE and the PS. In this scenario, the most appropriate model is in fact 1D with $\varepsilon = 1$. By ignoring the possible presence of this interface and multiple magnetization sources, we analyzed the long-t_m portion of the two-step spin-diffusion curve by throwing away the short-t_m portion, renormalizing and using the initial-rate approximation. In effect, we have computed the domain size for an assumed simple two-phase structure characterized by the spin-diffusion decay observed as the second step in the two-step decay curve. Using this approach, the phase-separated

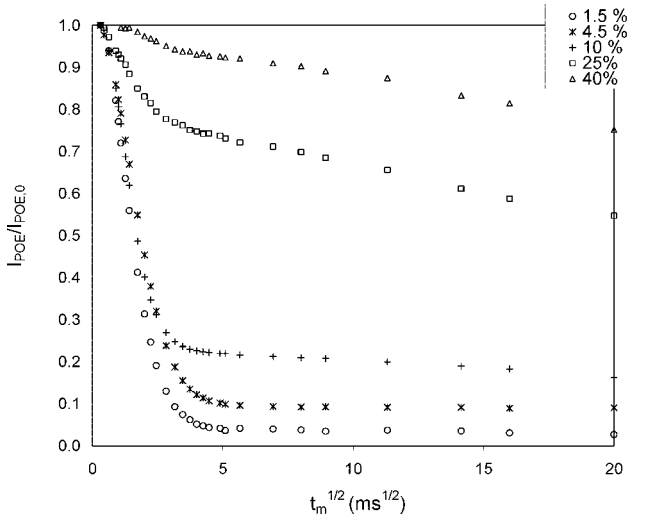

Figure 6. ^{1}H spin-diffusion curves for blends of PS with cPOE$_{400}$ at concentrations of 1.5, 4.5, 10, 25, and 40 wt %. The spin-diffusion curves plateau at end values representative of the POE-to-PS ^{1}H fractions in the samples. The curves for the 25 and 40 wt % blends consist of a fast and a slow decay, indicative of two separate POE domains in these samples.

POE is contained in domains with typical minimum dimensions of ~22 nm, which should be considered a very rough estimate. This is consistent with the DSC results (cf. Figure 2) that show only a part of the lPDME$_{500}$ component is dissolved into the PS and also with the ^{1}H line shapes that show two dynamically distinct domains for the lPDME$_{500}$ (cf. Figure 4a).

In addition to the data shown in Figure 5 for the 10 wt % blends of the smallest POE additives (cPOE$_{400}$, lPDME$_{500}$, and lPOE$_{400}$), spin-diffusion data were also collected for these blends at POE concentrations of 1.5, 4.5, 25, and 40 wt %. Spin-diffusion curves are shown in Figure 6 for the cPOE$_{400}$/PS blends as a function of cPOE$_{400}$ concentration. As the cPOE$_{400}$ concentration increases in the blend, the plateau values of the spin-diffusion curves increase which reflects the increasing fraction of POE-to-PS protons in the samples. The spin-diffusion curves in Figure 6 reveal single, small domains up to 10 wt % and two separate domains for 25 and 40 wt % cPOE$_{400}$. This is consistent with the DSC results (cf. Figure 2) which show complete dissolution of the cPOE$_{400}$ up to 10 wt %. The dissolved POE is present in the 25 and 40 wt % blends but is accompanied by phase-separated POE domains.

Domain sizes were calculated as described above and are summarized in Table 2 for all POE/PS blends. When the ^{1}H line shapes could be clearly resolved into two components, two spin-diffusion coefficients were determined from the respective T_2 relaxation data. In these cases of partially miscible blends, the spin-diffusion decay curve could be resolved into two components, and two domain sizes were computed and are reported for the dissolved POE and the phase-separated POE.

The blends can be placed into one of three categories according to the number and size of POE domains: completely miscible, partially miscible, and not miscible. The completely miscible blends are characterized by single, small domains attributed to dissolved POE. The completely immiscible blends are also characterized by single POE domains, but these POE domains are much larger due to phase separation of the POE. The partially miscible blends consist of two POE domains: a small one due to the dissolved POE and a larger one due to the phase-separated POE. The completely miscible blends are the ones prepared from cPOE$_{400}$ at concentrations ≤10 wt %. The dissolved POE domains in these completely miscible blends are 1−1.5 nm. The completely immiscible blends include all of the ones prepared with lPOE, lPDME$_{500}$ at 25 and 40 wt %, and with lPDME$_{2K}$ at 4.5 wt %. The POE domain sizes in these completely immiscible blends are ~100 nm and greater, indicative of gross phase separation. The partially miscible blends are those shown in Table 2, for which two POE domain sizes are reported. These include the cPOE$_{400}$ at 25 and 40 wt %, all the blends prepared with cPOE > 400 g/mol, the lPDME$_{500}$ at ≤10 wt %, and the lPDME$_{1K}$ at 4.5 wt %. These results are consistent with observations made upon solvent casting and annealing the sample films: the completely miscible blends were optically clear while the partially miscible and immiscible blends appeared varying degrees of cloudy.

For the completely miscible cPOE$_{400}$/PS blends (up to 10 wt %), the POE domain sizes are 1−1.5 nm. At these concentrations and for this molecular weight, the completely dissolved POE can exist as isolated molecules in the PS matrix; the overlap fraction for linear POE of 400 g/mol is about 0.25. Thus, these domain sizes should reflect some characteristic size of a cPOE$_{400}$ molecule. For 400 g/mol linear POE, the radius of gyration (R_g) was calculated to be 0.7 nm using a characteristic ratio of 5 and an average bond length of 1.46 Å. Since the R_g for a cyclic polymer is approximately half the value of the linear polymer of equivalent molecular weight,[66] the R_g for cPOE$_{400}$ is estimated to be 0.35 nm. This value seems reasonable when compared to some reported molecular dimensions of cPOE$_{440}$ (i.e., 30-crown-10); the crystal structure of cPOE$_{440}$ reveals a relatively flat extended molecule with no cavity that is 1.36 nm long and 0.4 nm wide.[67] Thus, we used the estimated R_g of 0.35 nm to calculate a relevant characteristic size for cPOE$_{400}$ as $2R_g$ = 0.7 nm, which is reasonably comparable to the 1.1 nm determined for the 1.5 wt % cPOE$_{400}$ blend by spin-diffusion NMR (see Table 2). This agreement suggests that the choice of $\varepsilon = 1$ may indeed be the most appropriate. The experimentally determined value may be even smaller than 1.1 nm. It has been reported recently that the local ^{1}H spin-diffusion coefficient for polystyrene is 0.2−0.3 nm^2/ms, significantly smaller than the 0.8 nm^2/ms typically used for rigid domains on the 10 nm length scale.[68] If we use 0.2 nm^2/ms for the D_{PS}, a d_{POE} of 0.9 nm is calculated for the 1.5 wt % cPOE$_{400}$ blend.

For higher concentrations and higher molecular weights, the size of the small (i.e., dissolved POE) domain increases. The small domain size in the cPOE$_{400}$/PS blends increases to 5 and then 8 nm for the 25 and 40 wt % blends, respectively. Thus, as the cPOE$_{400}$ concentration increases beyond 10 wt %, some degree of POE clustering (or interface broadening) takes place for the dissolved POE phase. An increase in the small domain size is also observed as larger POE molecules are used, for a given concentration. The dissolved POE domain size in the 4.5 wt % blends increases to 1.6 and then 3 nm for the cPOE$_{900}$ and cPOE$_{1.5K}$ blends, respectively. As the POE molecular weight increases, the POE solubility in PS decreases so that the small domains become increasingly POE-rich. This is consistent with the fact that the small domain sizes in the cPOE/PS blends do not scale proportionately with POE size, suggesting that the larger cPOE chains are not as swollen in the matrix as the smallest cPOE. This is also consistent with the reduction of the spin-diffusion coefficients (see Table 2) and ^{1}H line widths for the cPOE domains as the cPOE molecular weight increases, indicating higher mobility as the domains become more POE-rich.

The spin-diffusion coefficients (D_{POE}) shown in Table 2 reflect the changes observed in the POE segmental dynamics with morphology. Only three different D_{POE}'s are reported: 0.07 nm^2/ms for the dissolved POE, 0.01 nm^2/ms for the phase-separated POE in the partially miscible blends, and 0.007 nm^2/ms for the phase-separated POE in the completely immiscible blends. The D_{POE}'s are greatest for the dissolved POE since the POE

segmental dynamics are slowed by intimate contact with PS segments which makes the dipolar couplings strongest and spin diffusion more efficient. For example, the D_{POE} is 0.07 nm^2/ms for the completely miscible cPOE$_{400}$/PS blends at cPOE$_{400}$ concentrations $\leq$10 wt %. This value, 0.07 nm^2/ms, is exactly the same used for the POE phase in microphase-separated poly(styrene−ethylene oxide) diblock copolymers in which the POE segments are covalently linked to the PS segments.[69] For the partially miscible blends for which two spin-diffusion coefficients could be measured, the D_{POE} for dissolved POE is also 0.07 nm^2/ms, while the D_{POE} for the phase-separated POE domains is 0.01 nm^2/ms, reflecting the reduced dipolar couplings in these domains due to increased POE segmental mobility. For the completely immiscible blends, for example all of the lPOE/PS blends, the D_{POE} decreases to 0.007 nm^2/ms as gross phase separation further allows increased POE dynamics and reduced dipolar couplings. These D_{POE} data are consistent with the ^{1}H line shape data, as they should be since the D_{POE}s are determined from T_2 measurements that scale inversely with ^{1}H line widths.

The DSC results of Figure 2 indicate that all or some fraction of the cPOE$_{400}$ dissolves in PS to lower the blend T_g at concentrations of 1.5−40 wt %. The cPOE$_{400}$ domains responsible for this T_g depression range in size from 1 to 8 nm. For all of the other blends, the small POE domain is no larger than 5 nm (for the 4.5 wt % lPDME$_{1K}$/PS blend). For all of the blends, the phase-separated POE domain, or large domain in the case of two POE domains, is no smaller than ∼22 nm (21 nm for the 40 wt % cPOE$_{400}$/PS blend when $\varepsilon = 1$). Thus, 10−20 nm seems to be a critical size for the POE domain in these POE/PS blends. Below this critical size, the POE is intimately mixed with the PS, and segmental dynamics are influenced. Above this critical size, the POE is effectively phase separated and does not influence PS segmental dynamics. These conclusions are based on the results obtained from a combination of thermal analysis and solid-state NMR measurements on these polymer blends.

Scattering measurements would also be useful. Examples in the literature confirm that small-angle X-ray scattering (SAXS) and spin-diffusion NMR provide similar or complementary information.[29,57,70−73] This is not surprising since the commonly used spin-diffusion coefficients were established by conducting spin-diffusion experiments on samples with known domain sizes previously determined with SAXS.[25,28] For example, electron density correlation lengths computed from SAXS data agree with long periods determined from spin-diffusion NMR on samples of polyacrylonitrile threaded with cyclic POEs.[29] Domain size and size dispersion determined from SAXS and spin-diffusion NMR were found to agree for blends of cellulose and two different synthetic polymers.[70] Agreement between SAXS and spin-diffusion NMR data has also been reported for interdomain distances measured for a variety of copolymers.[71−73] When the two methods have not been in agreement, it was attributed to differences in the models used to analyze the two types of data[69] or to electron density fluctuations occurring on different length scales from those governed by the different chemical compositions of the two phases.[74] Scattering measurements on blends of PS with cyclic POE are in progress.

Conclusions

Hydroxyl-terminated linear poly(oxyethylene) (lPOE, 400−1500 g/mol) is not miscible in polystyrene (15 kg/mol) for concentrations $\leq$40 wt %. By replacing the hydroxyl end groups with methoxyl end groups, partially miscible blends can be formed at concentrations up to 4.5 wt % for 1 kg/mol and up to 10 wt % for 500 g/mol linear methoxyl-terminated POE. By cyclizing the POE, completely miscible POE/PS blends can be prepared at concentrations up to 10 wt % for 400 g/mol cyclic POE (cPOE). Higher concentrations and higher molecular weights of cyclic POE give partially miscible blends. For all concentrations and molecular weights studied, cyclic POE is more miscible in PS than linear POE. The miscibility of cyclic POE in PS is evidenced by a blend T_g that is reduced compared to the T_g of pure PS. For the miscible blends, a second T_g is observed below the blend T_g but much higher than the T_g of pure POE. This elevated POE T_g, which is consistent with recently reported dynamic confinement effects,[53] indicates the POE segmental dynamics are slowed in the blend compared to pure POE. This was confirmed with ^{1}H solid-state NMR line shape studies that revealed broader lines, indicative of reduced segmental dynamics, for the POE dissolved into the PS matrix.

Solid-state NMR spin-diffusion measurements were used to estimate the POE domain sizes in the blends. For the miscible blends and for the dissolved POE in the partially miscible blends, the POE domain sizes are in the range of 1−8 nm, with the smallest domains appearing for the smaller POE additives at the lower concentrations. Partial miscibility is marked by the appearance of second POE domains with sizes >∼20 nm, in which the POE exhibits increased segmental dynamics compared to the dissolved POE.

In summary, cyclization of poly(oxyethylene) can be used to prepare miscible blends of poly(oxyethylene) with polystyrene. These miscible blends exhibit heterogeneous dynamics on the nanometer length scale. Along with molecular weight and primary chemical structure, topology can be a useful tool in developing miscible polymer blends and broadening the palette of material properties available to designers, engineers, and formulators.

Acknowledgment. This work was supported by the National Science Foundation. We gratefully acknowledge contributions by Tiejun Zhao, Johannes Leisen, Angela Camp, and Lindsay Evans. Helpful discussions with David Bucknall and Klaus Schmidt-Rohr are appreciated.

References and Notes

(1) Yilmaz, E.; Yilmaz, O.; Caner, H. *Eur. Polym. J.* **1996**, *32* (8), 927–933.
(2) Abdel-Azim, A.-A.; Atta, A. M.; Farahat, M. S.; Boutros, W. Y. *J. Appl. Polym. Sci.* **1998**, *69*, 1471–1482.
(3) Ting, S. P.; Bulkin, B. J.; Pearce, E. M. *J. Polym. Sci., Polym. Chem.* **1981**, *19* (6), 1451–1473.
(4) Jin, X.; Zhang, S.; Runt, J. *Macromolecules* **2003**, *36* (21), 8033–8039.
(5) Pilar, J.; Sikora, A.; Labsky, J.; Schlick, S. *Macromolecules* **1993**, *26* (1), 137–143.
(6) Akiba, I.; Ohba, Y.; Akiyama, S. *Macromolecules* **1999**, *32* (4), 1175–1179.
(7) Anastasiadis, S. H.; Gancarz, I.; Koberstein, J. T. *Macromolecules* **1989**, *22* (3), 1449–1453.
(8) Orr, C. A.; Cernohaus, J. J.; Guegan, P.; Hirao, A.; Jeon, H. K.; Macosko, C. W. *Polymer* **2001**, *42*, 8171.
(9) Lebovitz, A. H.; Khait, K.; Torkelson, J. M. *Polymer* **2003**, *44*, 199–206.
(10) Cates, M. E.; Deutsch, J. M. *J. Phys. (Paris)* **1986**, *47*, 2121–2128.
(11) Santore, M. M.; Han, C. C.; McKenna, G. B. *Macromolecules* **1992**, *25* (13), 3416–3423.
(12) Zhao, T.; Beckham, H. W. *Polym. Prepr. (Am. Chem. Soc., Div. Polym. Chem.)* **2002**, *43* (1), 467–468.
(13) Kuo, C. M.; Clarson, S. J.; Semlyen, J. A. *Polymer* **1994**, *35* (21), 4623–4626.
(14) Kambour, R. P.; Nachlis, W. L.; Carbeck, J. D. *Polymer* **1994**, *35* (1), 209–211.
(15) Nachlis, W. L.; Bendler, J. T.; Kambour, R. P.; MacKnight, W. J. *Macromolecules* **1995**, *28* (23), 7869–7878.
(16) Khokhlov, A. R.; Nechaev, S. K. *J. Phys. (Paris)* **1996**, *6*, 1547–1555.
(17) Lee, M. H.; Fleischer, C. A.; Morales, A. R.; Koberstein, J. T.; Koningsveld, R. *Polymer* **2001**, *42*, 9163–9172.
(18) Qian, C.; Grigoras, S.; Kennan, L. D. *Macromolecules* **1996**, *29*, 1260–1265.

(19) Oike, H.; Imaizumi, H.; Mouri, T.; Yoshioka, Y.; Uchibori, A.; Tezuka, Y. *J. Am. Chem. Soc.* **2000**, *122* (40), 9592–9599.
(20) Kricheldorf, H. R.; Al-Masri, M.; Schwarz, G. *Macromolecules* **2002**, *35* (24), 8936–8942.
(21) Bielawski, C. W.; Benitez, D.; Grubbs, R. H. *Science* **2002**, *297*, 2041–2044.
(22) White, B. M.; Watson, P. W.; Barthelme, E. E.; Beckham, H. W. *Macromolecules* **2002**, *35* (14), 5345–5348.
(23) Singla, S.; Zhao, T.; Beckham, H. W. *Macromolecules* **2003**, *36* (18), 6945–6948.
(24) Wunderlich, B. *Macromolecular Physics*; Academic Press: New York, 1980.
(25) Clauss, J.; Schmidt-Rohr, K.; Spiess, H. W. *Acta Polym.* **1993**, *44*, 1–17.
(26) Schmidt-Rohr, K.; Spiess, H. W. *Multidimensional Solid-State NMR and Polymers*; Academic: New York, 1994.
(27) Mellinger, F.; Wilhelm, M.; Spiess, H. W.; Baumstark, R.; Haunschild, A. *Macromol. Chem. Phys.* **1999**, *200*, 719–730.
(28) Mellinger, F.; Wilhelm, M.; Spiess, H. W. *Macromolecules* **1999**, *32* (14), 4686–4691.
(29) Nagapudi, K.; Leisen, J.; Gibson, H. W.; Beckham, H. W. *Macromolecules* **1999**, *32* (9), 3025–3033.
(30) Viras, K.; Yan, Z. G.; Price, C.; Booth, C.; Ryan, A. J. *Macromolecules* **1995**, *28*, 104.
(31) Yu, G. E.; Sun, T.; Yan, Z. G.; Price, C.; Booth, C.; Cooke, J.; Ryan, A. *Polymer* **1997**, *38* (1), 35–42.
(32) Cooke, J.; Viras, K.; Yu, G. E.; Yonemitsu, T.; Ryan, A. J.; Price, C.; Booth, C. *Macromolecules* **1998**, *31*, 3030.
(33) Yang, Z.; Cooke, J.; Viras, K.; Ryan, A. J.; Gorry, P. A.; Booth, C. *J. Chem. Soc., Faraday Trans.* **1997**, *93*, 4033.
(34) Lutz, T. R.; He, Y.; Ediger, M. D.; Cao, H.; Lin, G.; Jones, A. A. *Macromolecules* **2003**, *36* (5), 1724–1730.
(35) Schantz, S. *Macromolecules* **1997**, *30*, 1419–1425.
(36) Zawada, J. A.; Ylitalo, C. M.; Fuller, G. G.; Colby, R. H.; Long, T. E. *Macromolecules* **1992**, *25* (11), 2896–2902.
(37) Shimada, S.; Kashima, K.; Hori, Y.; Kashiwabara, H. *Macromolecules* **1990**, *23* (16), 3769–3772.
(38) Miller, J. B.; McGrath, K. J.; Roland, C. M.; Trask, C. A.; Garroway, A. N. *Macromolecules* **1990**, *23* (21), 4543–4547.
(39) Roovers, J.; Toporowski, P. M. *Macromolecules* **1992**, *25* (13), 3454–3461.
(40) Kumar, S. K.; Colby, R. H.; Anastasiadis, S. H.; Fytas, G. *J. Chem. Phys.* **1996**, *105* (9), 3777–3788.
(41) Lodge, T. P.; Wood, E. R.; Haley, J. C. *J. Polym. Sci., Part B: Polym. Phys.* **2006**, *44*, 756–763.
(42) Dionísio, M.; Fernandes, A. C.; Mano, J. F.; Correia, N. T.; Sousa, R. C. *Macromolecules* **2000**, *33* (3), 1002–1011.
(43) Li, X.; Hsu, S. L. *J. Polym. Sci., Polym. Phys. Ed.* **1984**, *22*, 1331–1342.
(44) Goulart Silva, G.; Machado, J. C.; Somg, M.; Hourston, D. J. *J. Appl. Polym. Sci.* **2000**, *77*, 2034–2043.
(45) Smith, G. D.; Yoon, D. Y.; Jaffe, R. L.; Colby, R. H.; Krishnamoorti, R.; Fetters, L. J. *Macromolecules* **1996**, *29* (10), 3462–3469.
(46) Mark, J. E.; Flory, P. J. *J. Am. Chem. Soc.* **1965**, *87* (7), 1415–1423.
(47) Brandrup, J.; Immergut, E. H.; Grulke, E. A. *Polymer Handbook*, 4th ed.; Wiley-Interscience: New York, 1999.
(48) Smith, G. D.; Yoon, D. Y.; Jaffe, R. L. *Macromolecules* **1993**, *26* (19), 5213–5218.
(49) Miwa, Y.; Usami, K.; Yamamoto, K.; Sakaguchi, M.; Sakai, M.; Shimada, S. *Macromolecules* **2005**, *38* (6), 2355–2361.
(50) Genix, A.-C.; Arbe, A.; Alvarez, F.; Colmenero, J.; Willner, L.; Richter, D. *Phys. Rev. E* **2005**, *72*, 031808.
(51) Tyagi, M.; Arbe, A.; Colmenero, J.; Frick, B.; Stewart, J. R. *Macromolecules* **2006**, *39* (8), 3007–3018.
(52) Genix, A.-C.; Arbe, A.; Arrese-Igor, S.; Colmenero, J.; Richter, D.; Frick, B.; Deen, P. P. *J. Chem. Phys.* **2008**, *128*, 184901.
(53) Colmenero, J.; Arbe, A. *Soft Matter* **2007**, *3*, 1474–1485.
(54) Fox, T. G. *Bull. Am. Phys. Soc.* **1956**, *2*, 123.
(55) Frielinghaus, H.; Pedersen, W. B.; Larsen, P. S.; Almdal, K.; Mortensen, K. *Macromolecules* **2001**, *34* (4), 1096–1104.
(56) Li, K.-L.; Jones, A.; Inglefield, P. T.; English, A. D. *Macromolecules* **1989**, *22* (11), 4198–4204.
(57) VanderHart, D. L.; McFadden, G. B. *Solid State Nucl. Magn. Reson.* **1996**, *7*, 45–66.
(58) VanderHart, D. L. *Macromolecules* **1994**, *27* (10), 2837–2845.
(59) Matsumoto, A.; Egawa, Y.; Matsumoto, T.; Horii, F. *Polym. Adv. Technol.* **1996**, *8*(250−256).
(60) Asano, A.; Eguchi, M.; Shimizu, M.; Kurotsu, T. *Macromolecules* **2002**, *35* (23), 8819–8824.
(61) Hou, S.-S.; Chen, Q.; Schmidt-Rohr, K. *Macromolecules* **2004**, *37* (6), 1999–2001.
(62) Cho, G.; Natansohn, A. *Chem. Mater.* **1997**, *9* (1), 148–154.
(63) White, J. L.; Brant, P. *Macromolecules* **1998**, *31* (16), 5424–5429.
(64) Brus, J.; Dybal, J.; Schmidt, P.; Kratochvil, J.; Baldrian, J. *Macromolecules* **2000**, *33* (17), 6448–6459.
(65) Landfester, K.; Boeffel, C.; Lambla, M.; Spiess, H. W. *Macromolecules* **1996**, *29* (18), 5972–5980.
(66) Geyler, S.; Pakula, T. *Makromol. Chem., Rapid Commun.* **1988**, *9*, 617–623.
(67) Bheda, M. C.; Merola, J. S.; Woodward, W. A.; Vasudevan, V. J.; Gibson, H. W. *J. Org. Chem.* **1994**, *59* (7), 1694–1702.
(68) Chen, Q.; Schmidt-Rohr, K. *Solid-State Nuclear Magn. Reson.* **2005**, *29*, 142–152.
(69) Yu, H.; Natansohn, A.; Singh, M. A.; Torriani, I. *Macromolecules* **2001**, *34* (5), 1258–1266.
(70) VanderHart, D. L.; Manley, R. S. J.; Barnes, J. D. *Macromolecules* **1994**, *27* (10), 2826–2836.
(71) Yu, H.; Natansohn, A.; Singh, M. A.; Plivelic, T. *Macromolecules* **1999**, *32* (22), 7562–7571.
(72) Yu, H.; Wang, J.; Natansohn, A.; Singh, M. A. *Macromolecules* **1999**, *32* (13), 4365–4374.
(73) Wang, J.; Jack, K. S.; Natansohn, A. L. *J. Chem. Phys.* **1997**, *107* (3), 1016–1020.
(74) VanderHart, D. L.; Campbell, G. C.; Briber, R. M. *Macromolecules* **1992**, *25* (18), 4734–4743.

MA800327C